Electronic Supplementary Material (ESI) for Journal of Materials Chemistry A.
This journal is © The Royal Society of Chemistry 2022

Supporting Information

Ultra-low thermal conductivity in B_2O_3 composited SiGe bulk with enhanced thermoelectric performance at medium temperature region

Jian Nong,[†a] Ying Peng,[†b] Chengyan Liu,[a] Jin Bo Shen,[c] Qing Liao,[b] Yi Ling Chiew[d], Yoshifumi Oshima[d], Fu Cong Li[a], Zhong Wei Zhang[a], and Lei Miao[*a]

1. The Lorentz calculation

Because the charge carriers transport both heat and charge, κ_e is commonly estimated using the measured σ by the Wiedemann-Franz law: $\kappa_e=L\sigma T$, where L is the Lorenz number. Once κ_e is known, κ_l is computed by subtracting the κ_e from the total thermal conductivity, $\kappa=\kappa_e+\kappa_l$.

For a single parabolic band, L and S are both functions of reduced chemical potential (η) and carrier scattering factor (λ) only, the value of L is calculated according to the following formula:

$$L=\left(\frac{k_B}{e}\right)^2\frac{(1+\lambda)(3+\lambda)F_\lambda(\eta)F_{\lambda+2}(\eta)-(2+\lambda)^2F_{\lambda+1}(\eta)^2}{(1+\lambda)^2F_\lambda(\eta)^2}$$

$$S=\frac{k_B}{e}\left(\frac{(2+\lambda)F_{\lambda+1}(\eta)}{(1+\lambda)F_\lambda(\eta)}-\eta\right)$$

Where $F_j(\eta)$ represents the Fermi integral,

$$F_j(\eta)=\int_0^\infty\frac{\epsilon^j d\epsilon}{1+Exp[\epsilon-\eta]}$$

The Lorentz calculation values of different B_2O_3 adding amounts are shown in Fig. S1.

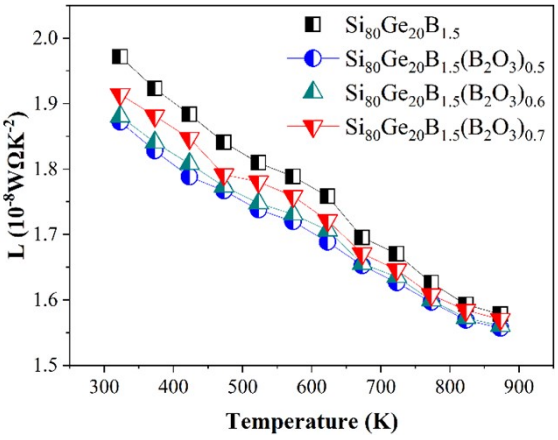

Fig. S1 Lorentz calculated value.

2. Effect of B_2O_3 on crystallization

In the miantext, it can be seen from XRD pattern, the stronger peaks intensities with the increase of the B_2O_3 content indicate that adding of B_2O_3 promotes the crystallization of SiGe. In addition to XRD characterization, we prepared samples without and added with B_2O_3 with the same sintering method and sintering time, and then characterized by SEM. As shown in Fig. S1(a), many holes and poor compactness in the sample without B_2O_3 are disclosed under the premise of the same preparation process. Figure S1(b) shows the sample added with B_2O_3, which has good porosity and compactness, further illustrating that B_2O_3 can promote crystallization.

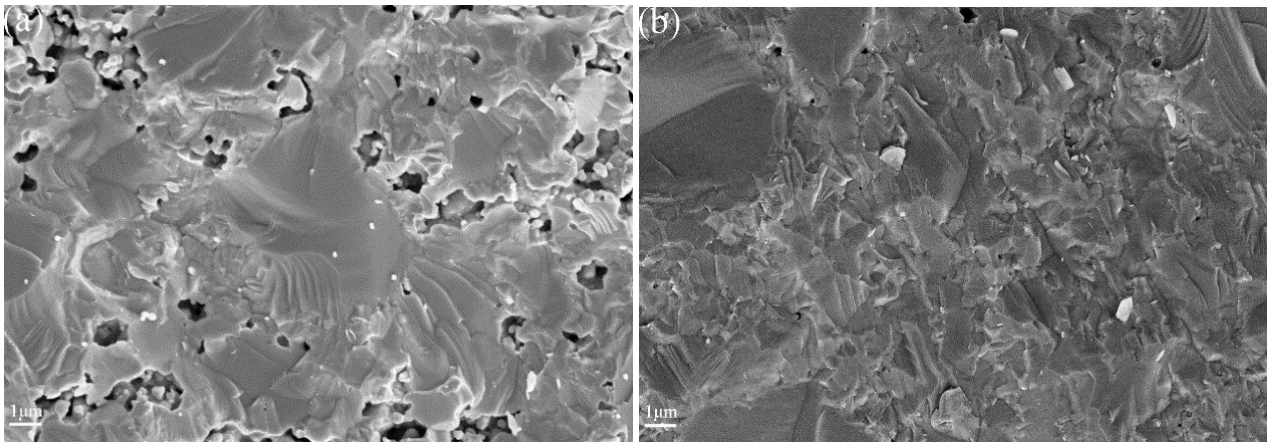

Fig. S2 (a) The SEM images of the sample without B_2O_3, (b) the SEM images of the sample added with B_2O_3

3. The EPMA measurement

EPMA works by bombarding micro-volume samples with focused electron beams and collecting X-rays emitted by various elements. Since the wavelengths of X-rays are characteristic of the emitting material, the sample components can be easily identified by recording wavelength dispersion spectra.

Figure. S3 is the EPMA test of $Si_{80}Ge_{20}B_{1.5}(B_2O_3)_{0.6}$ sample. It can be seen from the figure that the composition of point 1 and point 2 is different, and it can be judged that there are two phases. In addition, the sample was tested by surface scanning, and it was found that B element was distributed sporadically. It was inferred that it was probably a nano-second-phase containing B_2O_3, which needed to be further confirmed by TEM analysis.

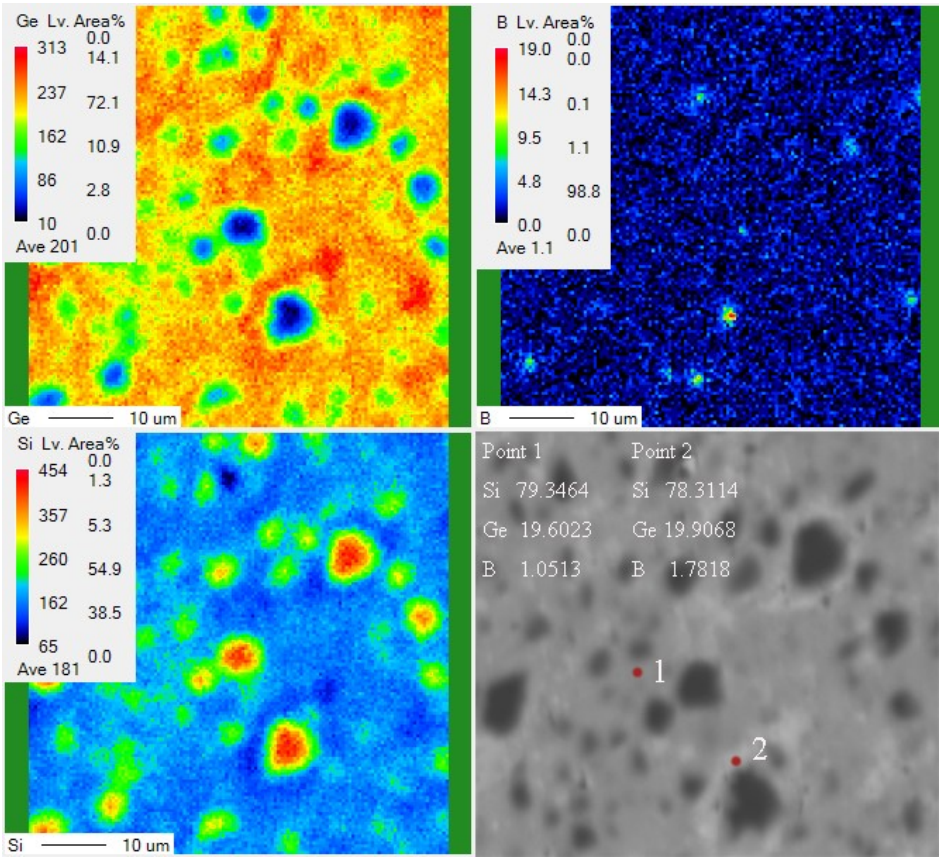

Fig. S3 The EPMA measurement of $Si_{80}Ge_{20}B_{1.5}(B_2O_3)_{0.6}$ Sample

4. The TEM observation

We have carried out TEM analysis in other different areas, and we can also find micropores, nano-second-phase, it is proved from the side that the micropores and the nano-second-phase are uniformly distributed.

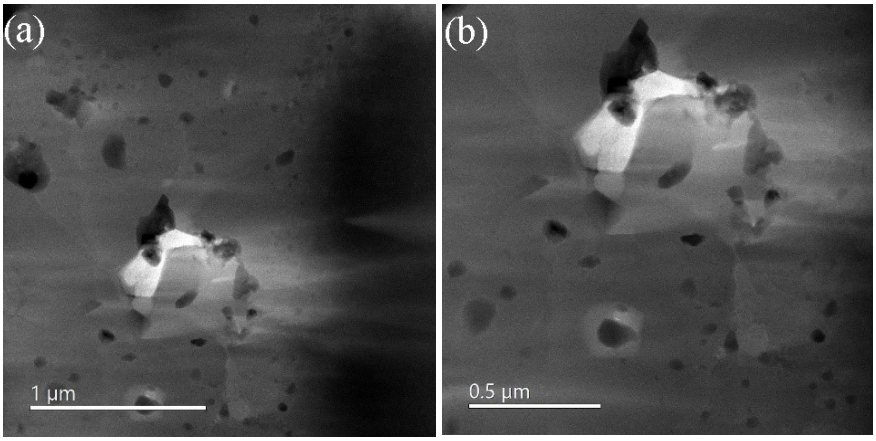

Fig. S4 TEM image of the micropores and nano-second-phase.

5. Fitting calculation of lattice thermal conductivity

We use the Callaway model to calculate the lattice thermal conductivity,[1-3] and the details are as follows.

$$k_l = \frac{k_B}{2\pi^2 v}\left(\frac{k_B T}{\hbar}\right)^3 \int_0^{\theta_D/T} \frac{x^4 e^x}{\tau_C^{-1}\left(e^x - 1\right)^2} dx$$

where x = ħω/(kBT), kB, ω, ħ, θD, v and τ_c^{-1} are the reduced phonon frequency, Boltzmann constant, phonon frequency, reduced Planck constant, Debye temperature, sound velocity and phonon-scattering relaxation time, respectively.

The relaxation time is affected by point defect scattering, phonon-phonon scattering, stacking fault and electron-phonon scattering, second phase, micropore and grain boundary scattering, as shown in the following formula.

$$\tau_c^{-1} = A\omega^4 + B\omega^2 T \exp\left(-\theta_D / 3T\right) + C\omega^2 + \frac{v}{d}$$

Among them, $A\omega^4$ corresponds to the relaxation time of the scattering of point defects, relaxation time of phonon-phonon scattering corresponding to $B\omega^2 T \exp\left(-\theta_D / 3T\right)$, $C\omega^2$ corresponds to the relaxation time of the stacking fault and electron-phonon scattering，$\frac{v}{d}$ corresponds to the relaxation time of the second phase, micropore and grain boundary scattering.

Combined with the actual test results and literature values,[4-8] we get the parameters of the following table. The d is obtained from the grain size distribution and micropore size distribution of TEM images, and the B is obtained by fitting with k_l known in previous studies. The point defect scattering is not considered, but only phonon-phonon scattering, electron-phonon scattering and boundary scattering are considered，by fitting the experimental k_l, C can be obtained when B is determined. On the premise that both B , C and d are determined, combined with the actual test results, A is calculated.

Table S1

Composition	A(s^3)	B(s/K)	C(s)	$\frac{v}{d}$ (s^{-1})
$Si_{80}Ge_{20}B_{1.5}$ $(B_2O_3)_{0.6}$	3500×10^{-45}	37×10^{-20}	0.4×10^{-17}	8×10^{9}

$Si_{80}Ge_{20}B_{1.5}$	1400×10^{-45}	37×10^{-20}	8×10^{-17}	2×10^{9}

References

1. S. A. Barczak, J. Buckman, R. I. Smith, A. R. Baker, E. Don, I. Forbes and J. G. Bos, *Materials (Basel)*, 2018, **11**, 1-13.
2. E. Lkhagvasuren, C. Fu, G. H. Fecher, G. Auffermann, G. Kreiner, W. Schnelle and C. Felser, *Journal of Physics D: Applied Physics*, 2017, **50**, 1-6.
3. S.-H. Lo, J. He, K. Biswas, M. G. Kanatzidis and V. P. Dravid, *Advanced Functional Materials*, 2012, **22**, 5175-5184.
4. Z. Liu, Q. Zhang, U. Wolff, C. G. F. Blum, R. He, A. Bahrami, M. Beier-Ardizzon, C. Reimann, J. Friedrich, H. Reith, G. Schierning and K. Nielsch, *ACS Appl Mater Interfaces*, 2021, **13**, 47912-47920.
5. X. Shi, Y. Pei, G. J. Snyder and L. Chen, *Energy & Environmental Science*, 2011, **4**, 4086-4095.
6. S. Wan, P. Qiu, X. Huang, Q. Song, S. Bai, X. Shi and L. Chen, *ACS Appl Mater Interfaces*, 2018, **10**, 625-634.
7. J. Yang, G. P. Meisner and L. Chen, *Applied Physics Letters*, 2004, **85**, 1140-1142.
8. T. Zhu, G. Yu, J. Xu, H. Wu, C. Fu, X. Liu, J. He and X. Zhao, *Advanced Electronic Materials*, 2016, **2**, 1-6.